Model Development for Piezoceramic Nanopositioners

Ralph C. Smith *, Andrew Hatch * and Tathagata De †

*Center for Research in Scientific Computation, North Carolina State University, Raleigh, NC 27695
†Electrical Engineering Department, Iowa State University, Ames, IA 50011

Abstract

In this paper, we develop nonlinear constitutive equations and resulting system models quantifying the nonlinear and hysteretic field-displacement relations inherent to piezoceramic elements employed in present nanopositioner designs. We focus specifically on piezoceramic rods utilizing d_{33} motion and piezoceramic shells driven in d_{31} regimes, but the modeling framework is sufficiently general to accommodate a variety of drive geometries. In the first step of the model development, lattice-level energy relations are combined with stochastic homogenization techniques to construct nonlinear constitutive relations which accommodate the hysteresis inherent to piezoceramic compounds. Secondly, these constitutive relations are employed in classical rod and shell relations to construct system models appropriate for presently employed nanopositioner designs.

1. Introduction

Pieozoceramic materials have been employed as actuators in scanning tunneling microscopes (STM) and atomic force microscopes (AFM) since their inception due to their high set point accuracy, large dynamic range, and relatively small temperature sensitivity [8]. More recent investigations have focused on the design of AFM stages for employment in applications ranging from nanoconstruction to the development of nuclear magnetic resonance microscopes (NMRM) with the goal of detecting single electron spins [6, 13, 20]. However, a fundamental challenge when employing piezoceramic actuators even at the low drive levels required for nanopositioning is the quantification and accommodation of hysteresis and constitutive nonlinearities inherent to the materials as depicted in Figure 1.

For certain drive regimes, the hysteresis and constitutive nonlinearities can be mitigated through either the drive electronics or feedback loops incorporated in the software. As detailed in [10, 11], the use of charge or current controlled amplifiers can essentially eliminate hysteresis. However, this mode of operation can be prohibitively expensive when compared with the more commonly employed voltage controlled amplifiers, and current control is ineffective if maintaining DC offsets as is the case when the x-stage of an AFM is held in a fixed position while a sweep is performed with the y-stage. For low scan rates, PID or robust control designs can be employed to accommodate hysteresis [4, 14]. However, at the high scan rates required for real-time product diagnostics or monitoring of biological processes, increasing noise-to-data ratios and diminishing high-pass characteristics of control filters preclude a sole reliance on feedback laws to eliminate hysteresis. This motivates the development of control designs which incorporate and approximately compensate for hysteresis through model inverses employed either in feedback or feedforward loops.

In this paper, we develop models for this purpose through a two step process. In the first step, Gibbs energy relations at the lattice level are minimized to provide models for the local average polarization generated by an applied field. The effects of material nonhomogeneities, polycrystallinity, and variable effective fields are subsequently incorporated through stochastic homogenization techniques to provide macroscopic constitutive relations which quantify the nonlinear and hysteretic field-polarization and field-strain behavior of the materials. In the second step of the development, these constitutive relations are incorporated in classical rod and shell theory to provide system models which quantify the displacements generated by prototypical nanopositioning designs.

To place this modeling framework in context, we compare it with the domain wall model employed in

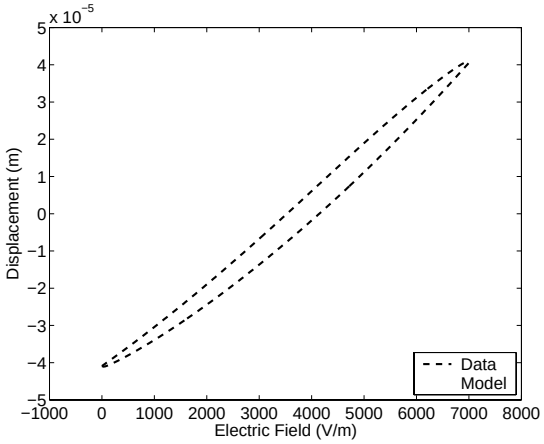

Figure 1. Quasistatic relation between the input field E and displacements generated by a PZT stacked actuator in an AFM stage.

[15] and Preisach model developed in [16] for characterizing the hysteretic behavior of nanopositioners. For certain choices of the Gibbs energy, the local polarization model in the present theory is the same as the anhysteretic relation in the domain wall theory. At the macroscopic level, however, the two models differ significantly – from the perspective of implementation, the present theory guarantees the closure of biased minor loops whereas this is accomplished in the domain wall model only if *a priori* knowledge of turning points is available. Furthermore, it is illustrated in [18] that the present theory provides an energy basis for extended Preisach models which enforces deletion but not congruency. Through the energy derivation, the proposed theory inherits several of the advantages associated with extended Preisach frameworks while avoiding the disadvantages associated with temperature, frequency and stress-dependent parameters.

We consider two motivating geometries for the model development. The first encompasses PZT rods of the type employed in AFM stages having the design depicted in Figure 2(a). In this case, strains are generated through d_{33} mechanisms which translate to longitudinal rod displacements. Appropriate 1-D constitutive relations are developed in Section 2.1 and the corresponding system model is constructed in Section 3.1. The second geometry is comprised of a PZT shell in which longitudinal, or z, displacements are generated through d_{31} mechanisms – see Figure 2(b). The 2-D constitutive relations and system model for this case are respectively developed in Sections 2.2 and 3.2.

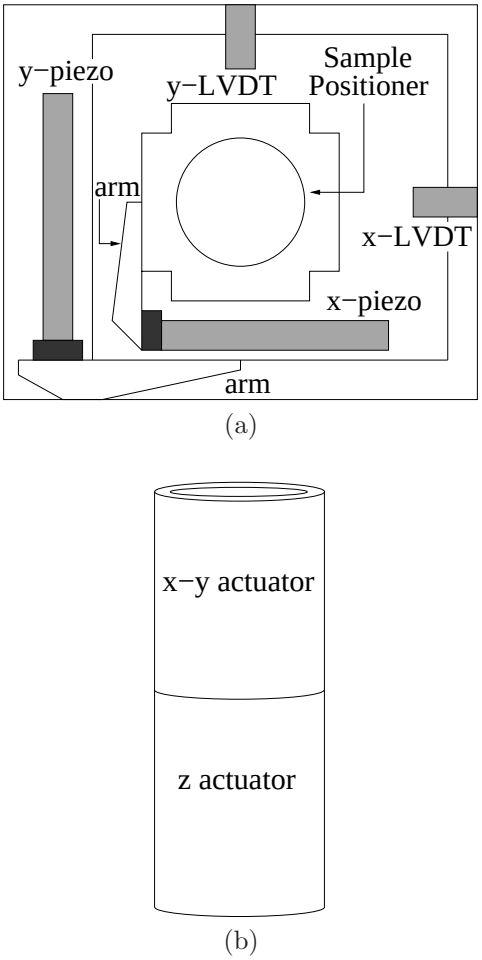

Figure 2. Actuator configurations employed for sample positioning in AFM. (a) Stacked actuators employed as x- and y-stages, and (b) cylindrical PZT transducer.

2. Constitutive Relations

When modeling the constitutive behavior of piezoceramic rods and shells, we assume linear stress-strain and strain-displacement relations in accordance with classical theory. Furthermore, both classical theory, [3, 9], and recent experiments have demonstrated that in the biased regimes used to obtain bidirectional strains, the relation between the polarization P and strains ε is approximately linear, and we retain that assumption throughout the development. At all drive levels, however, the map between applied voltages V or fields E and the polarization is nonlinear and hysteretic, and it is the quantification of these inherent properties which differentiates the proposed models from classical linear theory for piezoceramic rods and shells.

2.1. 1-D Constitutive Relations

The 1-D constitutive relations necessary for characterizing the strains generated by PZT rods follows from the general theory developed in [19] for quantifying the hysteresis and constitutive nonlinearities inherent to ferroelectric compounds. We summarize here those aspects of the theory pertinent to the development of PZT stages employed in nanopositioning devices.

It is illustrated in [19] that for stress-free, fixed temperature conditions, the piecewise quadratic Helmholtz energy relation

$$\psi(P) = \begin{cases} \frac{1}{2}\eta(P+P_R)^2 & , \ P \le -P_I \\ \frac{1}{2}\eta(P-P_R)^2 & , \ P \ge P_I \\ \frac{1}{2}\eta(P_I-P_R)\left(\frac{P^2}{P_I}-P_R\right) & , \ |P|<P_I \end{cases} \tag{1}$$

quantifies the internal energy derived under the assumption that dipoles are either aligned with the applied field or diametrically opposite to it. As depicted in Figure 3, P_I and P_R respectively denote the inflection point and polarization at which the positive local minimum of ψ occurs. The point P_R is also the local remanence polarization at the domain level. Finally, the fact that η is the reciprocal of the slope in the E-P relation after switching can be utilized to determine initial parameter values when constructing the model for a given piezoceramic compound and application.

To incorporate elastic interactions and ferroelectric coupling, we also consider the extended Helmholtz re-

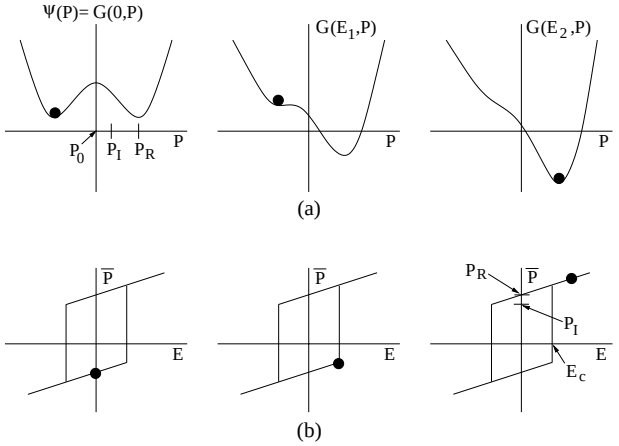

Figure 3. (a) Helmholtz energy ψ and Gibbs energy G for $\sigma = 0$ and increasing fields E. (b) Dependence of the local polarization $\overline{P}$ on the field E at the lattice level in the absence of thermal activation.

lation

$$\psi_e(P,\varepsilon) = \psi(P) + \frac{1}{2}Y^P\varepsilon^2 - Y^M\gamma\varepsilon P \qquad (2)$$

where Y^P denotes the Young's modulus at constant polarization and γ is an electromechanical coupling coefficient.

To accommodate applied stresses and fields, we employ the Gibbs energy relation

$$G(E,P,\varepsilon) = \psi(P) + \frac{1}{2}Y^P\varepsilon^2 - Y^M\gamma\varepsilon P - EP - \sigma\varepsilon \quad (3)$$

which incorporates the electrostatic, electromechanical and elastic energy relations.

For operating regimes in which thermal relaxation mechanisms are significant, the local average polarization at the lattice level is quantified by balancing the thermal and Gibbs energies through the Boltzmann distribution

$$\mu(G) = Ce^{-GV/kT} \qquad (4)$$

where μ specifies the probability of achieving an energy level G, C is a constant of integration, V is a reference volume and k is Boltzmann's constant. For brevity, we omit this case here and refer the reader to [19] for details concerning the extension of the constitutive relations to include thermal relaxation mechanisms.

For regimes in which thermal relaxation is negligible, the local average polarization $\overline{P}$ at the lattice level is determined by the necessary conditions

$$\frac{\partial G}{\partial P} = 0 \quad , \quad \frac{\partial^2 G}{\partial P^2} > 0. \qquad (5)$$

This yields the piecewise linear relation

$$[\overline{P}(E,\varepsilon;E_c,\xi)](t) = \begin{cases} [\overline{P}(E,\varepsilon;E_c,\xi)](0) \\ \frac{E}{\eta-2Y^P\gamma\varepsilon} - \frac{P_R\eta}{\eta-2Y^P\gamma\varepsilon} \\ \frac{E}{\eta-2Y^P\gamma\varepsilon} + \frac{P_R\eta}{\eta-2Y^P\gamma\varepsilon} \end{cases} \qquad (6)$$

for the respective cases $\{\tau(t) = \emptyset\}$, $\{\tau(t) \neq \emptyset$ and $E(\max\tau(t)) = -E_c\}$, $\{\tau(t) \neq \emptyset$ and $E(\max\tau(t)) = E_c\}$. The local coercive field is given by

$$E_c = \eta(P_R - P_I). \qquad (7)$$

The transition points τ are specified by

$$\tau(t) = \{t \in (0,T_f] \,|\, E(t) = -E_c \text{ or } E(t) = E_c\},$$

and

$$[\overline{P}(E,\varepsilon;E_c,\xi)](0) = \begin{cases} \frac{E}{\eta-2Y^P\gamma\varepsilon} - \frac{P_R\eta}{\eta-2Y^P\gamma\varepsilon} \\ \xi \\ \frac{E}{\eta-2Y^P\gamma\varepsilon} + \frac{P_R\eta}{\eta-2Y^P\gamma\varepsilon} \end{cases}$$

denotes the initial dipole orientation for respective initial fields $\{E(0) \leq -E_c\}$, $\{-E_c < E(0) < E_c\}$ or $\{E(0) \geq E_c\}$.

The local relation (6) quantifies the hysteretic relation between E and P for homogeneous, single crystal compounds having uniform effective field $E_e = E$. To extend this mesoscopic model to macroscopic regimes involving nonhomogeneous, polycrystalline compounds with variable effective fields, we consider certain parameters to be manifestations of underlying distributions rather than constant values.

Effective field effects (see [1]) are incorporated by assuming that the field at the lattice level is normally distributed about the applied field E with the density

$$\widehat{f}(E_e) = c_1 e^{-(E_e-E)^2/\bar{b}} \qquad (8)$$

where c_1 and $\bar{b}$ are positive constants. To incorporate variations in the lattice structure, we assume that the local coercive field E_c, specified by (7), is either normally or lognormally distributed. In the former case, it will exhibit a density f analogous to (8) whereas in the latter case, it has the density

$$f(E_c) = c_2 e^{-\ln(E_c/\bar{E}_c)/2b]^2}$$

where, if b is small compared with $\bar{E}_c$, $\bar{E}_c$ denotes a mean coercive field at which dipoles switch.

The macroscopic polarization model is then

$$P(E) = C\int_0^\infty \int_{-\infty}^\infty \overline{P}(E,\varepsilon;E_c,\xi) f(E_c)\widehat{f}(E_e)\, dE_e dE_c \qquad (9)$$

where $\overline{P}$ is given by (6). It is detailed in [18] that the formulation (9) provides an energy basis for certain Preisach representations with the difference that temperature and frequency dependencies are incorporated in the kernel of (9) rather than the parameters as is the case for Preisach models.

The elastic constitutive relation, in the absence of internal damping, is determined from the equilibrium conditions

$$\frac{\partial G}{\partial \varepsilon} = 0 \quad , \quad \frac{\partial^2 G}{\partial \varepsilon^2} > 0$$

which yields

$$\sigma = Y^P\varepsilon - Y^P\gamma P.$$

To incorporate Kelvin-Voigt damping, we posit that stress is proportional to a linear combination of strain, strain rate and polarization which yields the 1-D constitutive equation

$$\sigma = Y^P \varepsilon + c^P \dot{\varepsilon} - Y^P \gamma P \tag{10}$$

where c^P denotes the damping parameter at fixed polarization. In combination with (9), the constitutive relation (10) quantifies the material behavior in operating regimes dominated by uniaxial dynamics as is the case for PZT rods employed in the x- and y-stages of several present AFM designs.

2.2. 2-D Constitutive Relations

The constitutive behavior of a PZT shell employed for nanopositioning differs from that of the rod in two fundamental aspects: (i) the longitudinal actuation is due to d_{31} rather than d_{33} mechanisms, and (ii) longitudinal and circumferential stresses and strains are coupled due to the curvature (e.g., see [2]). The nature of the actuation simply yields a different electromechanical coupling coefficient which we denote by β in this case. To designate the coupled material behavior, we let ε_x, σ_x and $\varepsilon_\theta, \sigma_\theta$ respectively denote the normal strains and stresses in the longitudinal and circumferential directions and we denote shear strains and stresses by $e_{x\theta}$ and $\sigma_{x\theta}$. Finally, we let ν denote the Poisson ratio for the material.

To simplify the discussion, we consider the development of constitutive relations in the absence of internal damping and refer the reader to [2, 7, 15] for the extensions necessary to incorporate Kelvin-Voigt damping. With Y^P again denoting the Young's modulus, appropriate 2-D constitutive equations are

$$\begin{aligned}
\sigma_x &= \frac{Y^P}{1-\nu^2}(e_x + \nu e_\theta) - \frac{Y^P \beta}{1-\nu} P(E) \\
\sigma_\theta &= \frac{Y^P}{1-\nu^2}(e_\theta + \nu e_x) - \frac{Y^P \beta}{1-\nu} P(E) \\
\sigma_{x\theta} &= \sigma_{\theta x} = \frac{Y^P}{2(1+\nu)} e_{x\theta} \\
P(E) &= C \int_0^\infty \int_{-\infty}^\infty \overline{P}(E, \varepsilon; E_c, \xi) f(E_c) \widehat{f}(E_e)\, dE_e dE_c
\end{aligned} \tag{11}$$

with $\overline{P}$ specified in (6). These relations are employed when constructing the shell models in Section 3.2.

3. System Models

It was noted in Section 1 that two actuator geometries commonly employed for nanopositioning are piezoceramic rods and piezoceramic shells. In this section, we construct system models for these configurations based on the 1-D and 2-D constitutive relations developed in Section 2.

3.1. Stacked Actuator

When modeling the stacked actuator employed in the x- and y-stages of an AFM, we make the assumption that the cross-sectional area A is small compared with the length ℓ and we consider only longitudinal displacements u having the spatial coordinate x. In accordance with present stage design, one end of the rod is assumed fixed while the other encounters resistance due to the connecting mechanisms. We assume that this contribution can be modeled as a damped elastic system with mass M_L, stiffness k_L and damping coefficient c_L. The density of the stacked actuator is denoted by ρ and the Young's modulus and Kelvin-Voigt damping coefficients are again denoted by Y^P and c^P.

Force balancing along the stacked actuator yields the relation

$$\rho A \frac{\partial^2 u}{\partial t^2} = \frac{\partial \mathcal{N}}{\partial x} \tag{12}$$

where the resultant $\mathcal{N} = \int_A \sigma dA$ is given by

$$\mathcal{N} = c^P A \frac{\partial u}{\partial x} + c_D A \frac{\partial^2 u}{\partial x \partial t} - c^P A \gamma P(E)$$

once the linear relation $\varepsilon = \frac{\partial u}{\partial x}$ is employed for the strains. The nonlinear and hysteretic map between input fields E and the polarization P is specified by (9). The fixed-end condition yields $u(t,0) = 0$ and balancing forces at $x = \ell$ yields

$$\mathcal{N}(t,\ell) = -k_L u(t,\ell) - c_L \frac{\partial u}{\partial t}(t,\ell) - M_L \frac{\partial^2 u}{\partial t^2}(t,\ell).$$

Finally, initial conditions are taken to be $u(0,x) = \frac{\partial u}{\partial t}(0,x) = 0$.

The relation (12) along with the boundary conditions provides a strong form of the stacked actuator model. For numerical implementation, it is advantageous to reduce smoothness requirements on approximating elements through consideration of a weak form of the model obtained either through Hamiltonian principles or integration by parts. Details regarding the derivation of a weak form for an analogous magnetostrictive rod, and a description of the resulting ODE system obtained through a finite element discretization of this weak model, are provided in [5].

The performance of the model is illustrated in Figure 4 where the model prediction is compared with quasistatic AFM data collected at 0.28 Hz. For the model construction, normal densities f and $\hat{f}$ were employed when quantifying the coercive and effective field distributions. It is observed that the model accurately quantifies the hysteresis loss and hence will eliminate the delay associated with uncompensated hysteresis in present control designs.

3.2. Cylindrical Actuators

Secondly, we consider the development of a model for the cylindrical transducer depicted in Figure 2(b).

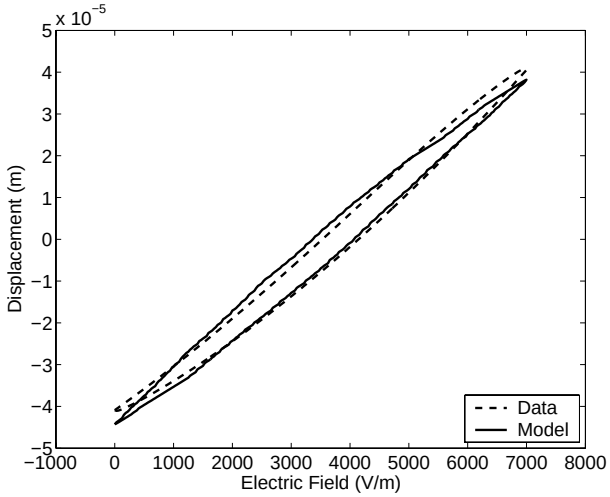

Figure 4. Quasistatic experimental data from the AFM stage depicted in Figure 2(a) and model prediction.

We focus on the actuator employed for z-displacements since real-time control of this component is required to maintain constant forces between the sample and micro-cantilever. The mass of the shell employed for x-y translation is combined with the mass of the sample to provide an inertial force acting on the free end of the z-actuator.

For modeling purposes, we assume that the shell has length ℓ, thickness h, and radius R. The axial direction is specified along the z-axis and the longitudinal, circumferential and transverse displacements are respectively denoted by u, v and w. The density and Young's modulus are respectively designated by ρ and Y^P, and the region occupied by the middle surface of the shell is specified by $\Gamma_0 = [0, \ell] \times [0, 2\pi]$. We consider the case in which the bottom edge of the shell ($x = 0$) is clamped and the opposite end ($x = \ell$) is acted upon only by the inertial force associated with the combined mass m of the x-y actuator and the sample. Finally, we simplify the discussion by considering the model development in the absence of internal damping. The extensions necessary to incorporate Kelvin-Voigt damping can be incorporated by assuming that stress is a linear combination of strain, strain rate and polarization as detailed in [2, 15].

As detailed in [2], force and moment balancing yield the Donnell-Mushtari shell equations

$$R\rho h\frac{\partial^2 u}{\partial t^2} - R\frac{\partial \mathcal{N}_x}{\partial x} - \frac{\partial \mathcal{N}_{x\theta}}{\partial \theta} = 0$$

$$R\rho h\frac{\partial^2 v}{\partial t^2} - \frac{\partial \mathcal{N}_\theta}{\partial \theta} - R\frac{\partial \mathcal{N}_{x\theta}}{\partial x} = 0$$

$$R\rho h\frac{\partial^2 w}{\partial t^2} - R\frac{\partial^2 \mathcal{M}_x}{\partial x^2} - \frac{1}{R}\frac{\partial^2 \mathcal{M}_\theta}{\partial \theta^2} - 2\frac{\mathcal{M}_{x\theta}}{\partial x \partial \theta} + \mathcal{N}_\theta = 0$$

where $\mathcal{N}_x, \mathcal{N}_\theta$ and $\mathcal{N}_{x\theta}$ are general force resultants and $\mathcal{M}_x, \mathcal{M}_\theta$ and $\mathcal{M}_{x\theta}$ are moment resultants. The boundary conditions at the fixed end $x = 0$ are taken to be

$$u = v = w = \frac{\partial w}{\partial x} = 0,$$

and the conditions

$$\mathcal{N}_x = -m\frac{\partial^2 u}{\partial t^2} \quad , \quad \mathcal{N}_{x\theta} + \frac{\mathcal{M}_{x\theta}}{R} = 0$$

$$\mathcal{Q}_x + \frac{1}{R}\frac{\partial \mathcal{M}_{x\theta}}{\partial \theta} = 0 \quad , \quad \mathcal{M}_x = 0$$

are enforced at $x{=}\ell$. The first resultant condition incorporates the inertial force due to the mass of the piezoceramic cylinder employed for y-z translation along with the mass of the sample.

The force and moment resultants are specified by integrating the stress relations (11), or the product of the stress and moment arm, through the thickness of the shell. In the absence of shear stresses, this yields

$$\mathcal{N}_x = \frac{Y^P h}{1-\nu^2}(e_x + \nu e_\theta) - \frac{Y^P h\beta}{1-\nu}P(E)$$

$$\mathcal{N}_\theta = \frac{Y^P h}{1-\nu^2}(e_\theta + \nu e_x) - \frac{Y^P h\beta}{1-\nu}P(E)$$

$$\mathcal{N}_{x\theta} = \frac{Y^P h}{2(1+\nu)}e_{x\theta}$$

and

$$\mathcal{M}_x = \frac{Y^P h^3}{12(1-\nu^2)}(\kappa_x + \nu\kappa_\theta) - \frac{Y^P h^3\beta}{12(1-\nu)}P(E)$$

$$\mathcal{M}_\theta = \frac{Y^P h^3}{12(1-\nu^2)}(\kappa_\theta + \nu\kappa_x) - \frac{Y^P h^3\beta}{12(1-\nu)}P(E)$$

$$\mathcal{M}_{x\theta} = \frac{Y^P h^3}{24(1+\nu)}\tau.$$

The midsurface strains and changes in curvature are given by

$$e_x = \frac{\partial u}{\partial x} \quad , \qquad \kappa_x = -\frac{\partial^2 w}{\partial x^2}$$

$$e_\theta = \frac{1}{R}\frac{\partial v}{\partial \theta} + \frac{w}{R} \quad , \qquad \kappa_\theta = -\frac{1}{R^2}\frac{\partial^2 w}{\partial \theta^2} \qquad (13)$$

$$e_{x\theta} = \frac{\partial v}{\partial x} + \frac{1}{R}\frac{\partial u}{\partial \theta} \quad , \qquad \tau = -\frac{2}{R}\frac{\partial^2 w}{\partial x \partial \theta}.$$

As with the stacked actuator, it is advantageous to consider a weak form of the model when developing approximation techniques. Details regarding this development can be found in [2, 7].

4. Concluding Remarks

In this paper, we have developed 1-D and 2-D constitutive relations quantifying the nonlinear and hysteresis behavior of PZT transducers employed in present nanopositioner designs. These constitutive relations are then combined with classical rod and shell theory to provide models which quantify the displacements generated by stacked and cylindrical PZT actuators. This provides a design tool for future actuator design as well as a framework amenable to inversion as a prelude to control design employing approximate inverse filters to compensate for the hysteresis and constitutive nonlinearities inherent to the materials [12].

Acknowledgments

This research was supported in part by the Air Force Office of Scientific Research under the grant AFOSR-F49620-01-1-0107, the NSF grants CMS-0099764 and CMS-0201560, and the DARPA MOSAIC Program through the grant 1000-G-CF980.

References

[1] J.C. Anderson, *Dielectrics*, Reinhold Publishing Corporation, New York, 1964.

[2] H.T. Banks, R.C. Smith and Y. Wang, *Smart Material Structures: Modeling, Estimation and Control*, Masson/John Wiley, Paris/Chichester, 1996.

[3] W.G. Cady, *Piezoelectricity*, McGraw-Hill, New York, 1946.

[4] D. Croft, G. Shed and S. Devasia, "Creep, hysteresis, and vibration compensation for piezoactuators: Atomic force microscopy application," *Journal of Dynamic Systems, Measurement, and Control*, 23, pp. 35-43, 2001.

[5] M.J. Dapino, R.C. Smith and A.B. Flatau, "A structural strain model for magnetostrictive transducers," *IEEE Transactions on Magnetics*, 36(3), pp. 545-556, 2000.

[6] DARPA Program on Molecular Observation, Spectroscopy and Imaging Using Cantilevers (MOSAIC), http://www.darpa.mil/dso/thrust/biosci/mosaic.htm.

[7] R.C.H. del Rosario and R.C. Smith, *Spline approximation of thin shell dynamics,* International Journal for Numerical Methods in Engineering, 40, pp. 2807-2840, 1997.

[8] P.K. Hansma, V.B. Elings, O. Marti and C.E. Bracker, "Scanning tunneling microscopy and atomic force microscopy: Application to biology and technology," *Science*, 242, pp. 209-242, 1988.

[9] T. Ikeda, *Fundamentals of Piezoelectricity*, Oxford University Press, Oxford, 1990.

[10] J.A. Main, E. Garcia and D.V. Newton, "Precision position control of piezoelectric actuators using charge feedback," *Journal of Guidance, Control, and Dynamics.* 18(5), pp. 1068-73, 1995.

[11] J.A. Main, D. Newton, L. Massengil and E. Garcia, "Efficient power amplifiers for piezoelectric applications," *Smart Materials and Structures*, 5(6), pp. 766-775, 1996.

[12] J. Nealis and R.C. Smith, "Model-based robust control design for magnetostrictive transducers operating in hysteretic and nonlinear regimes," CRSC Technical Report CRSC-TR03-25; *IEEE Transactions on Automatic Control*, submitted.

[13] D. Rugar, O. Züger, S.T. Hoen, C.S. Yannoni, H.-M. Vieth and R.D. Kendrick, "Force detection of nuclear magnetic resonance," *Science*, 264, p. 1560, 1994.

[14] S. Salapaka, A. Sebastian, J.P. Cleveland and M.V. Salapaka, "High bandwidth nano-positioner: A robust control approach," *Review of Scientific Instruments*, 73(9), pp. 3232-3241, 2002.

[15] R.C. Smith and M. Salapaka, "Model development for the positioning mechanisms in an atomic force microscope," *International Series of Numerical Mathematics*, Vol 143, pp. 249-269, 2002.

[16] R.C. Smith, M.V. Salapaka and L. Cherveny, "A Preisach model for quantifying hysteresis in an atomic force microscope," Proceedings of the SPIE, Smart Structures and Materials 2002, Volume 4693, pp. 498-504, 2002.

[17] R.C. Smith, M.V. Salapaka, A. Hatch, J. Smith and T. De, "Model development and inverse compensator design for high speed nanopositioning," Proc. 41st IEEE Conf. Dec. and Control, 2002, Las Vegas, NV.

[18] R.C. Smith and S. Seelecke, "An energy formulation for Preisach models," Proceedings of the SPIE, Smart Structures and Materials 2002, Volume 4693, pp. 173-182, 2002.

[19] R.C. Smith, S. Seelecke, Z. Ounaies and J. Smith, "A free energy model for hysteresis in ferroelectric materials," CRSC Technical Report CRSC-TR03-01; *Journal of Intelligent Material Systems and Structures*, to appear.

[20] S.A. Wolf, D.D. Awschalom, R.A. Buhrman, J.M. Daughton, S. von Molnár, M.L. Chtchelkanova and D.M. Teger, "Spintronics: A spin-based electronics vision for the future," *Science*, 294, p. 1488-1495, 2001.